Acta of Bioengineering and Biomechanics
Vol. 17, No. 4, 2015

Original paper
DOI: 10.5277/ABB-00128-2014-04

Skinfold creep under load of caliper. Linear visco- and poroelastic model simulations

JOANNA NOWAK[1]*, BARTOSZ NOWAK[2], MARIUSZ KACZMAREK[1]

[1] Institute of Mechanics and Applied Computer Science, Kazimierz Wielki University Bydgoszcz, Poland.
[2] Faculty of Civil Engineering, Bauhaus-Universität Weimar, Weimar, Germany.

Purpose: This paper addresses the diagnostic idea proposed in [11] to measure the parameter called rate of creep of axillary fold of tissue using modified Harpenden skinfold caliper in order to distinguish normal and edematous tissue. Our simulations are intended to help understanding the creep phenomenon and creep rate parameter as a sensitive indicator of edema existence. The parametric analysis shows the tissue behavior under the external load as well as its sensitivity to changes of crucial hydro-mechanical tissue parameters, e.g., permeability or stiffness. Methods: The linear viscoelastic and poroelastic models of normal (single phase) and oedematous tissue (two-phase: swelled tissue with excess of interstitial fluid) implemented in COMSOL Multiphysics environment are used. Simulations are performed within the range of small strains for a simplified fold geometry, material characterization and boundary conditions. The predicted creep is the result of viscosity (viscoelastic model) or pore fluid displacement (poroelastic model) in tissue. Results: The tissue deformations, interstitial fluid pressure as well as interstitial fluid velocity are discussed in parametric analysis with respect to elasticity modulus, relaxation time or permeability of tissue. The creep rate determined within the models of tissue is compared and referred to the diagnostic idea in [11]. Conclusions: The results obtained from the two linear models of subcutaneous tissue indicate that the form of creep curve and the creep rate are sensitive to material parameters which characterize the tissue. However, the adopted modelling assumptions point to a limited applicability of the creep rate as the discriminant of oedema.

Key words: *computer simulations, soft tissue, lymphoedema, viscoelasticity, poroelasticity, modeling*

1. Introduction

A treatment of breast cancer causing disturbance in lymph transport from interstitial space through lymphatic system to blood can result in accumulation of lymph in tissue of trunk and arm [10]. A simple measure used in evaluation of swelling of the posterior axillary tissue is based on the comparison of thickness of the tissue's fold on the normal and affected sides. The alternative measure, as proposed in [11], may constitute a comparison of change of thickness of the fold of such tissues determined at two characteristic time instants under approximately constant load exerted by modified Harpenden skinfold calliper. The authors of [11] determined the time instants (10 s and 60 s), the optimum loads (37 kPa) due to the action of the calliper's spring and made series of tests confirming differences in the behaviour of normal and affected tissue. The phenomenon which is considered as responsible for the thickness changes is creep phenomenon of tissue. Since the tissue with edema contains more interstitial fluid than the normal tissue [8], the observed creep is usually larger in the former case. While this original idea is very interesting for clinicians the literature confirming the possibility of axillary edema assessment throughout analysis of creep is very limited and this is a possible reason that this simple methodology is not widely used. The creep phenomenon of the lymphedematous tissue was also mentioned in papers [3] and [13], where another diagnostic method, called indentation test or tonometry, was considered. The results indicated greater sensitivity of response of lymphedema-

* Corresponding author: Joanna Nowak, Institute of Mechanics and Applied Computer Science, Kazimierz Wielki University, Kopernika 1, 85-074 Bydgoszcz, Poland. Tel: +48 252 325-76-53, e-mail: joanna_n@ukw.edu.pl
Received: July 7th, 2014
Accepted for publication: January 12th, 2015

tous tissue to mechanical load than observed in the normal tissue.

This paper presents results of simulations of the creep of a skinfold assuming two mechanical models of tissue: viscoelastic and poroelastic one. Assuming that normal tissue can be modelled as a viscoelastic material and the edematous tissue is a fluid saturated porous material the models are considered in order to explore possible behaviour of normal and edematous skinfold. The influence of material properties characterising the tissue on mechanical and hydro-mechanical processes under constant stress imposed by calliper tips is analysed. This parametric analysis may deliver better knowledge on possible sources of lack of success of the creep measure in diagnostic practice.

We assume simplified linear models of soft tissue with homogeneous and isotropic material properties. This means that the presence of skin is not incorporated. Additionally the fold geometry as well as boundary conditions are idealized and the symmetry of the process is assumed. The load level considered is almost five times lower than the originally applied in [11] in order to limit the resultant strain which has to be acceptable within geometrically linear models. The control time instants are the same as found in [11].

The discussion of results obtained by finite element method is concentrated on tissue deformations, interstitial fluid pressure, and fluid velocity. The deformation of tissue under calliper tips represents the creep phenomenon due to internal friction or displacement of interstitial fluid. The analysis refers to control points located beneath and next to the loading domain. Parametric analysis reveals the role of elasticity modulus, viscosity of permeability of tissue for creep behaviour.

2. Materials and methods

In Fig. 1, a picture of a patient with truncal lymphoedema tested with modified Harpenden skinfold caliper and a simplified geometry of the skinfold which is used in simulations are shown.

The soft tissue is modeled as the viscoelastic or poroelastic material. Only in the latter case the presence of interstitial fluid is represented explicitly by the pore fluid which saturates porous skeleton. In both cases we assume negligible role of inertial and gravity forces as well as the symmetry of stress tensor. Similar level of complexity (number of model parameters) is postulated within the constitutive mechanical relationships of the models applied. The presence of skin, inhomogeneity and anisotropy of the material are disregarded.

2.1. Viscoelastic model

A single phase viscoelastic model of solid material which incorporates the assumptions introduced is based on the equilibrium equation

$$\nabla \cdot \boldsymbol{\sigma} = \mathbf{0} \tag{1}$$

where $\boldsymbol{\sigma}$ is the stress tensor. Following the concept of the generalized Maxwell model of the viscoelastic continuum with internal variables [2], the stress tensor is decomposed into volumetric stress (pressure) P and stress deviator $\mathbf{s}$

$$\boldsymbol{\sigma} = -\mathrm{P}\mathbf{I} + \mathbf{s} \tag{2}$$

and then the constitutive relationships for the linear viscoelastic material are written as the equations

$$\begin{gathered} \mathrm{P} = -K\varepsilon_v, \quad \mathbf{s} = 2G\boldsymbol{\varepsilon}_d + \sum_{j=1}^{n} 2G_j \mathbf{q}_j, \\ \frac{d\mathbf{q}_j}{dt} + \frac{1}{\tau_j}\mathbf{q}_j = \frac{d\boldsymbol{\varepsilon}_d}{dt}, \end{gathered} \tag{3}$$

where the strain tensor $\boldsymbol{\varepsilon}$ defined by the displacement vector $\mathbf{u}$ is decomposed into volumetric strain $\varepsilon_v = tr\boldsymbol{\varepsilon}$ and tensor of strain deviator $\boldsymbol{\varepsilon}_d$ as follows $\boldsymbol{\varepsilon} = \frac{1}{2}[(\nabla \mathbf{u})$

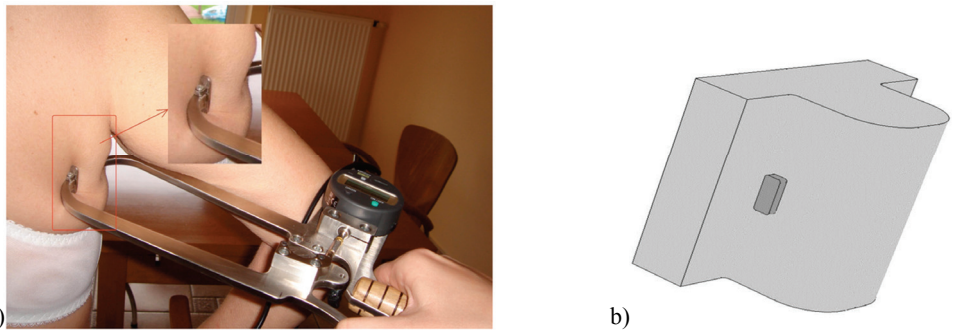

a) b)

Fig. 1. A test with the modified Harpenden caliper [9] (a) and simplified geometry of the skinfold used in simulations (b)

$+ (\nabla \mathbf{u})^T] = \frac{1}{3}\varepsilon_v \mathbf{I} + \boldsymbol{\varepsilon}_d$; $K = \frac{EG}{3(3G-E)}$ is the bulk modulus, G is the shear modulus, E stands for Young's modulus, G_j represent stiffness of arms (j = 1, ..., n) in the generalized Maxwell model, $\mathbf{q}_j$ denote the symmetric tensors of internal state (internal strains) and τ_j are relaxation times [2]. In the applied model of tissue the simplest approximation is considered, i.e., i = 1, which guarantees similar complexity of the viscoelastic and poroelastic models.

2.2. Poroelastic model

The poroelastic model of soft tissue is based here on Biot's formulation [4] and comprises the equilibrium equation of the two phase system and Darcy's law, i.e.,

$$\nabla \cdot \boldsymbol{\sigma} = \mathbf{0}\,, \tag{4}$$

$$\mathbf{q} = -\frac{k}{\eta}\nabla \mathrm{p}\,, \tag{5}$$

where now $\boldsymbol{\sigma}$ denotes the total stress (sum of the stress in solid and fluid phase), $\mathbf{q}$ is the discharge velocity of pore fluid with respect to solid skeleton, p stands for pore pressure, k and η denote permeability of porous medium and dynamic viscosity of fluid.

The linear constitutive relationships for mechanical behaviour of fluid saturated porous material are the following

$$\boldsymbol{\sigma} + \alpha \mathrm{p}\mathbf{I} = 2\mu\boldsymbol{\varepsilon} + \lambda\varepsilon_v\mathbf{I}\,, \tag{6}$$

$$\zeta = \frac{1}{M}p + \alpha\varepsilon_v\,, \tag{7}$$

where ζ denotes the change of fluid content in porous matrix, $\mu = G$ and λ are Lame elastic constants of drained porous matrix describing response of solid skeleton in terms of the effective stress to the applied strain, α is the volumetric coupling coefficient, and M is the elasticity constant relating the change of fluid content and pore pressure, [4].

From equilibrium equation (4) and constitutive relation (6) we have

$$\eta\nabla^2\mathbf{u} + (2\mu+\lambda)\nabla\cdot(\nabla\mathbf{u}) - \alpha\nabla p = 0\,. \tag{8}$$

Since the change in fluid content ζ can be expressed by the product of porosity ϕ and difference of dilatations of pore fluid θ and solid matrix ε_v, i.e.,

$$\zeta = \phi(\theta - \varepsilon_v)\,, \tag{9}$$

and the linearized dependence of the divergence of discharge velocity can be represented as

$$\nabla\cdot\mathbf{q} = \phi\frac{\partial}{\partial t}(\theta - \varepsilon_v)\,, \tag{10}$$

combining equations (5), (7) and (10) we can write

$$\frac{1}{M}\frac{\partial p}{\partial t} + \nabla\cdot\left(-\frac{k}{\eta}\nabla p\right) - \alpha\frac{\partial}{\partial t}\varepsilon_v = 0\,. \tag{12}$$

Expressing the Lame constants by Young's modulus E and Poisson's ratio ν of drained material $\mu = \frac{E}{2(1+\nu)}$, $\lambda = \frac{E\nu}{2(1+\nu)(1-2\nu)}$ and representing parameter M for incompressible matrix material as $M = \frac{K_f}{\phi}$, [4], where K_f denotes the fluid compressibility, we get the following coupled system of equations of the poroelastic model

$$\frac{E}{2(1+\nu)}\nabla^2\mathbf{u} + \frac{E}{2(1+\nu)(1-2\nu)}\nabla\cdot(\nabla\mathbf{u}) - \alpha\nabla p = 0) \tag{13}$$

$$\frac{\phi}{K_f}\frac{\partial p}{\partial t} + \nabla\cdot\left(-\frac{k}{\eta}\nabla p\right) + \alpha\frac{\partial}{\partial t}\nabla\cdot\mathbf{u} = 0\,. \tag{14}$$

Equations (13), (14) will be used to model the behavior of subcutaneous tissue as fluid saturated porous material in terms of matrix displacement $\mathbf{u}$ and pore pressure p.

2.3. Model parameters, initial and boundary conditions

Table 1 lists the parameters characterizing the skinfold geometry and material properties of the tissue assumed for simulations.

Due to the symmetry of the mechanical problem of the loaded skinfold only half of the fold, shown in Fig. 1b, with the adjacent tissue is taken into account. The geometry of this part of the fold and the cross-section are shown in Fig. 2. The length, width and half of the thickness of the simulated fold are L = 8 cm, W_f = 6 cm and d = 2 cm while the width and thickness of the adjacent tissue are W_t = 6 cm and D = 2 cm. The rectangular coordinate system is used with x axis oriented along the fold. The load p_c = 7.8 kPa is applied to the surface of contact of skin with the caliper tip. The geometrical parameters for the caliper tips are selected following paper [11]. The size of the tip is characterized by length l = 15 mm and width w = 6 mm. Then, the surface area of the contact is equal to

Table 1. Geometrical and material parameters assumed for simulations

Parameter	Description	Value	Units
L	Length of fold	8.0	cm
W_f	Width of fold	6.0	cm
W_t	Width of adjacent tissue layer	6.0	cm
d	Thickness of half of the fold	2.0	cm
D	Thickness of tissue layer	2.0	cm
a	Depth of control points	0.05	cm
b	Distance between control points	1.0	cm
l	Length of caliper tip	1.5	cm
w	Width of caliper tip	0.6	cm
α	Volumetric coupling coefficient	1.0	–
ρ	Liquid density	1000.0	kg/m^3
ν	Poisson's number of the tissue	0.33	–
E	Young's modulus of the tissue	2/2.5/3 × 10^4	Pa
ϕ	Porosity	0.05	–
K_f	Liquid compressibility	2.3 × 10^9	Pa
k	Hydraulic permeability	0.5/1.5/4.5 × 10^{-13}	m^2
η	Dynamic viscosity	0.001	Pas
p_c	Mechanical load (normal stress)	7.78 (58, 32)	kPa (mmHg)
G_1	Parameter of stiffness in Maxwell model	3.6	kPa
τ_1	Relaxation time in Maxwell model	3/7/16	s

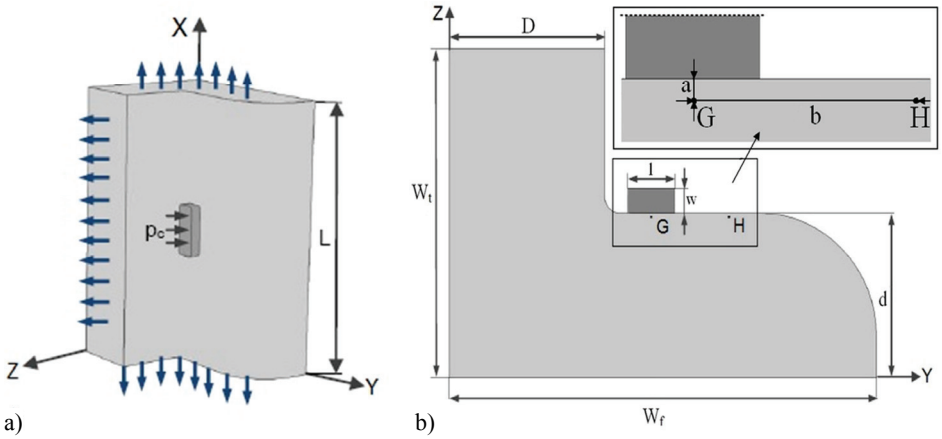

Fig. 2. Geometry of half of the fold (a) and cross-section through the element (b)

90 mm^2. The assumed load on caliper tips is about five times lower than the value considered in [11]. The values of basic material parameters characterizing mechanical and hydraulic properties of soft tissue are adopted from literature, see [1], [6]–[8], [12] and were discussed in [7]. The parametric analysis is performed for a range of model parameters being deviations from their basic values and ensuring that results of simulations satisfy the accepted limitations. Studies of the poroelastic model with respect to variation of stiffness of tissue assume three values of drained Young's modulus $E = 2/2.5/3 \times 10^4$ kPa and the same for each case drained Poisson's ratio $\nu = 0.33$, while the possible range of hydraulic properties of tissue is expressed by the three values of permeability which are $k = 0.5/1.5/4.5 \times 10^{-13}$ m^2. The studies of the viscoelastic model assume elastic parameters (E, G) the same as the drained elastic parameters of the poroelastic model. The other two coefficients of the Maxwell model (G_1, τ) are selected to ensure that the predictions for initial deformation level and rate of creep are comparable for the viscoelastic and the poroelastic models. As a result, the parameter of stiffness of an arm in Maxwell model $G_1 = 3.6$ kPa, and the values of relaxation time $\tau = 3/7/16$ s.

Initially the pore fluid pressure and tissue displacement are assumed to be equal to zero. The relative fluid flow is not allowed through skin and symmetry planes. The displacements of tissue for boundaries which are included by symmetry planes are equal to zero.

3. Results

The results of numerical simulations of the skinfold behavior under load of caliper using the above formulated models and the finite element method are implemented in COMSOL Multiphysics environment is presented in the next few figures. Two control points G and H, located in different parts of the fold (see Fig. 2b), are selected in order to study the skinfold behavior. The points are placed 0.5 mm (in Fig. 2b distance a) beneath the surface of the fold. Point G is located just below the center of the caliper tip while point H is placed next to the tip, 1 cm (distance b) from point G (see Fig. 2b).

(a) Parametric analysis for 3D geometry

The evolution (time dependence) of tissue displacement, pore pressure and pore fluid velocity for selected model parameters (given in Table 1) are studied. As in paper [11], the change of thickness of the fold at two time instants (10 s and 60 s) are compared to estimate the creep rate parameters. Figures 3, 4 and 5 show displacements of tissue at control points G and H as functions of time predicted by the viscoelastic and poroelastic models. The level of deformation at the point beneath the caliper tips (G) for all the cases considered is few times larger than for the tissue next to the tips (H).

The displacements under the tip (point G) depend visibly on Young's modulus while next to the tip (point H) the dependence is less pronounced, see Fig. 3. The slope of creep curves obtained in the case of the viscoelastic model (Fig. 3a) is similar to that obtained from the poroelastic model (Fig. 3b).

The plots in Fig. 4 visualize the dependence of tissue displacement on factors that influence the fold's creep: permeability and relaxation time. The form of time dependence of displacement predicted by both models at the same control points are different although the levels of values are comparable. The displacements under the tip are about five times greater than next to the tip.

The results obtained within the viscoelastic model show that the rate of deformation in the observation window is greater for lower values of relaxation time. Given the values of relaxation time 3, 7, and 16 s the

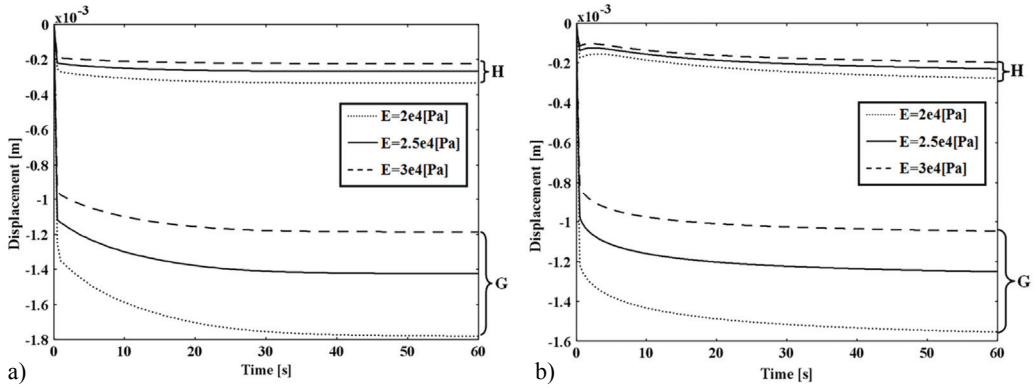

Fig. 3. Dependence of tissue displacement on time at control points G and H for the viscoelastic model (a) and the poroelastic model (b) and selected values of Young's modulus

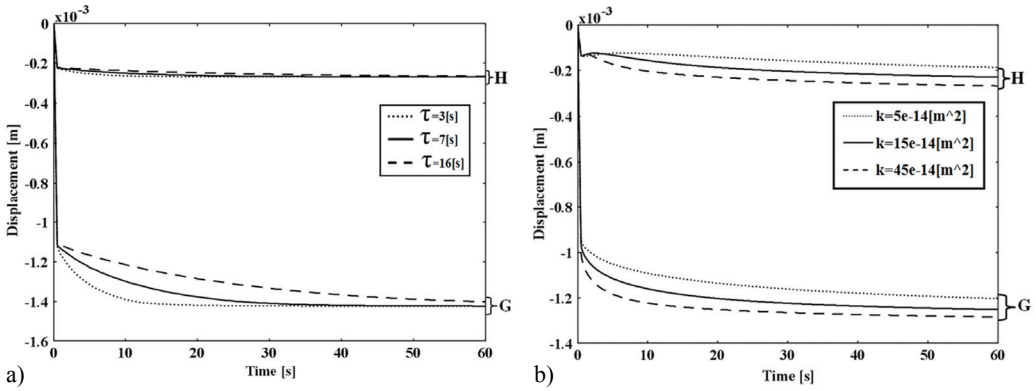

Fig. 4. Dependence of tissue displacement on time at control points G and H for the viscoelastic model (a) and the poroelastic model (b) assuming different values of relaxation time and permeability

creep rate parameter as defined in [11] amounts to 0.034, 0.125, and 0.187 mm, respectively. The deformation process reaches equilibrium after about 22, 42 and 86 s.

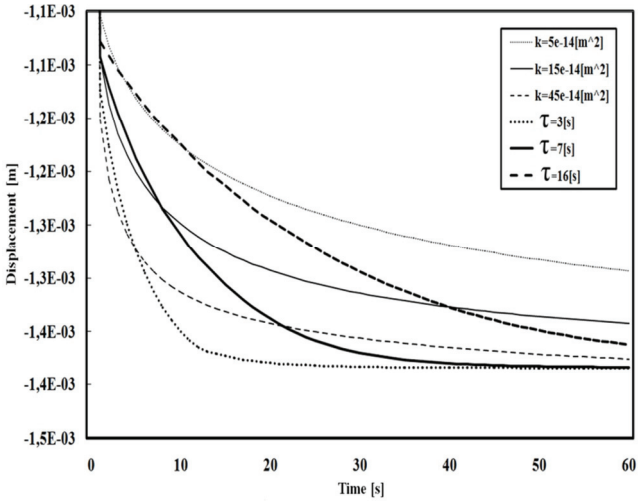

Fig. 5. Comparison of tissue displacement as a function of time at control point G for the viscoelastic and poroelastic models assuming different values of relaxation time and permeability

For the poroelastic model the rate of deformation increases with the values of permeability. The values of the creep rate for permeability 5, 15, and 45 10^{-14} mm^2 are 0.117, 0.094, and 0.0062 mm, respectively, and for all the cases the deformation does not stabilize within the range of observation (60 s). At point H the sensitivity of deformation with respect to relaxation time is lower than with respect to permeability. The effect is related to outflow of fluid from the loaded domain to its vicinity. Higher permeability causes that interstitial fluid flows out faster from the tissue, therefore the material can deform easier and the time which is necessary to reach the equilibrium state is shorter.

For better visualization of the difference between creep of skinfold predicted by the two models considered, displacements at point G are compared in Fig. 5. The adopted values of parameters of stiffness ensure comparable initial displacement of tissue for the viscoelastic and the poroelastic models. The permeability and the relaxation time influence the form of the creep curves and duration of the process. The initial high rate of deformation of the fold is comparable for both

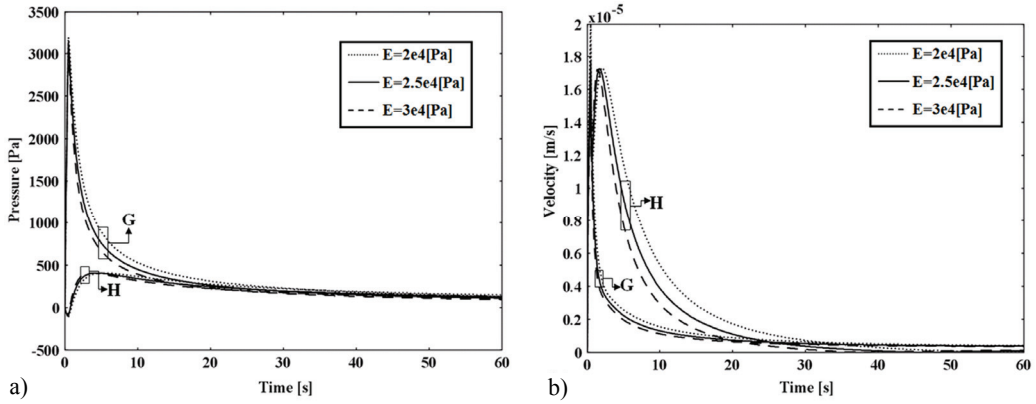

Fig. 6. Dependence of pore fluid pressure (a) and velocity (b) on time at points G and H for different Young's moduli

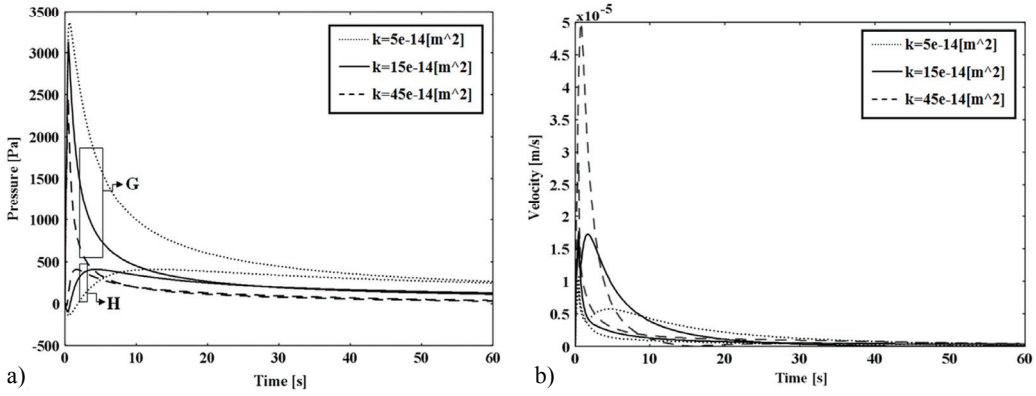

Fig. 7. Dependence of pore pressure (a) and velocity (b) on time for different values of permeability at control points G and H

models. Then, the rate predicted by the poroelastic model slows down compared to the one obtained from the viscoelastic model. The observed behavior can be explained by the fact that initially the pore fluid is relatively fast squeezed out from the tissue beneath the tips to the unloaded domain surrounding tips because the pressure gradient is high. In the second period the pore pressure gradient becomes more homogeneous (this is visible in Fig. 8a) and lower while the rate of fluid outflow from the loaded tissue slows down.

The results shown in Fig. 6 and 7 concern parametric studies of the poroelastic model for changes in pore pressure and fluid velocity under caliper tip (point G) and next to the tip (point H) as a function of time. Different values of Young's modulus (E = 2, 2.5, and 3 × 10^4 Pa) and identical permeability (k = 1.5 × 10^{-13} m^2), Fig. 6, or constant Young's modulus (E = 2.5 × 10^4 Pa) and different values of permeability (k = 5, 15 and 45 × 10^{-14} m^2), Fig. 7, are considered.

The results show significant difference of pressure values at control points in the initial period (approx. 10 s), Fig. 6a. Because of the possibility of expansion of tissue next to the caliper tips the pressure in this part is much lower than under the tips, although the distance is only 1 cm. The same effect induces that the lower the Young's modulus is, the lower the pressure is observed. Within the observation time range considered the pressure dissipates almost to zero.

The changes in pore fluid velocity at control points, see Fig. 6b, show weak dependence on Young's modulus. Moreover, it is seen that the velocity approaches fast the values close to zero. The pore fluid velocity in tissue next to the tip (point H) has longer non-zero values and is more dependent on Young's modulus of tissue than the fluid velocity at point G.

The results shown in Fig. 7a and 7b refer to parametric studies of influence of permeability on pore pressure and pore fluid velocity in tissue under caliper tip (point G) and next to the tip (point H).

The lower the permeability, the higher the pore pressure is present both under the tip (point G) and in the vicinity (point H). This behavior is physically well justified because of easier fluid outflow in the cases of higher permeability. Only for the highest permeability full dissipation of pore pressure is possible within 60 s. The above explanation is supported by the dependence of pore fluid velocity on tissue permeability, Fig. 7b, and the fact that the flow becomes relatively slow for low permeability tissue. The velocity is particularly high in the initial time period and at point H is significantly higher than at point G.

b) Spatial distributions for 2D geometry, comparison with the 3D case

The longitudinal shape of the skinfold and caliper tips is justified in spite of the simulations for 3D cases performing calculations for 2D geometry. Then, the infinite size of the fold and tips is assumed and simulations are noticeably less time consuming. The complexity of the solution for 3D geometry had significant influence on the number of mesh elements and the

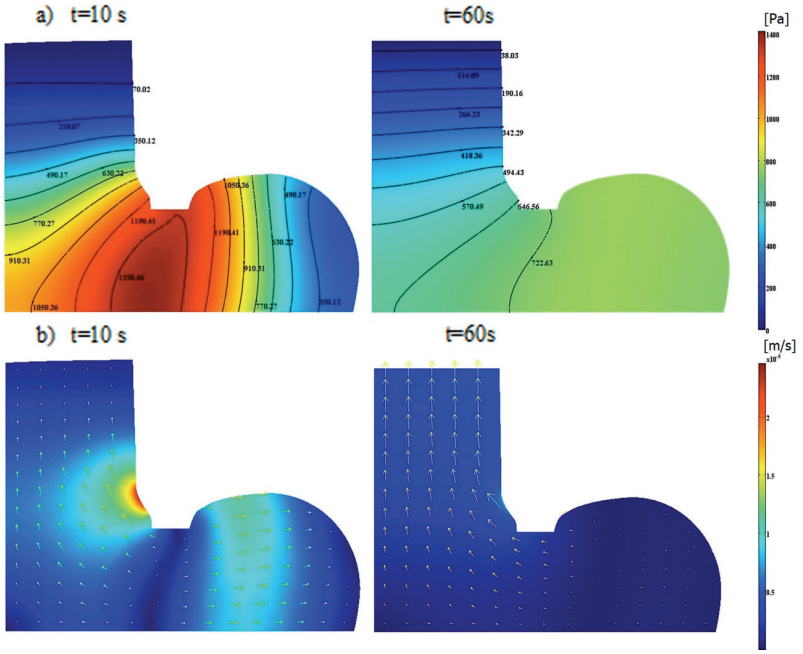

Fig. 8. Spatial distributions of pore pressure (a) and fluid velocity (b) for loaded skinfold (7.78 kPa) and two time instants 10 and 60 s (poroelastic model)

calculation time. Typically, in the 2D case the number of mesh elements was three times lower and the calculation time ten times shorter than for the 3D case.

Spatial distributions of pore pressure and pore fluid velocity obtained from 2D poroelastic model for time instants 10 and 60 s are shown in Fig. 8.

The evolution of pore pressure and fluid velocity at control points G and H derived from 2D and 3D cases are compared in Fig. 9. The results showing high pore pressure for 10 s in the loaded area of tissue indicate that initially the pore fluid takes on most of the load from caliper tips. The pressure is particularly high under and in the vicinity of tips. With time the pressure goes down and for 60 s it is approximately three times smaller than the maximum value. The process is related to evacuation of pore fluid from loaded domain, which is visible on plots presenting pore fluid velocity distributions (Fig. 8a). The pore pressure next to the tips (point H) is initially low and increases up to values comparable with pressure at point G, see Fig. 9a. The process could be explained by redistribution of pore fluid and limited deformation of tissue matrix next to the tips.

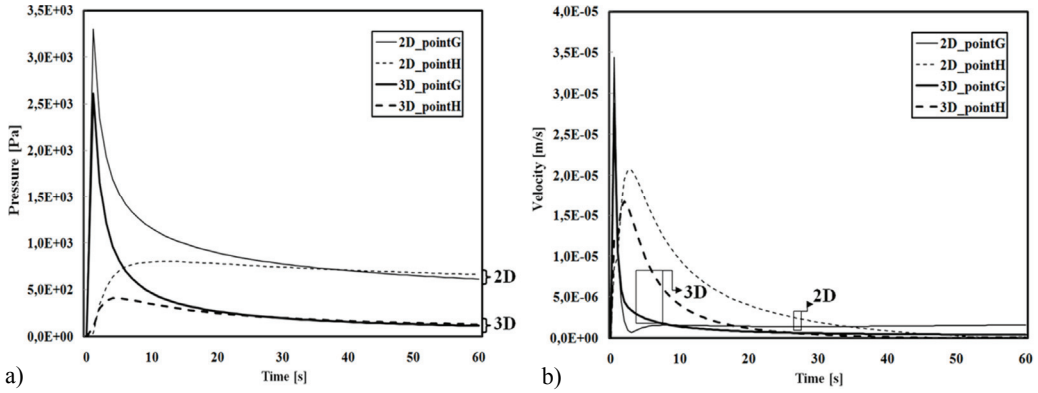

Fig. 9. Comparison of pore pressure (a) and fluid velocity (b) at control points. The results are obtained from 2D and 3D simulations within the poroelastic model

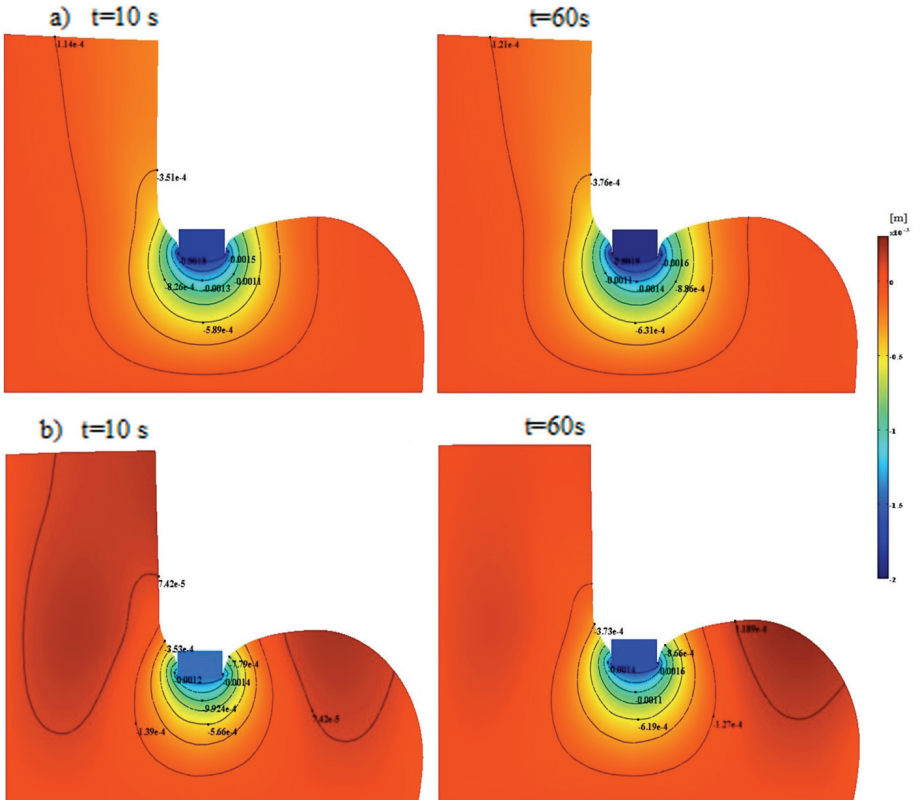

Fig. 10. Spatial distributions of tissue displacement from the viscoelastic (a) and the poroelastic (b) models for time instants 10 and 60 s

In Fig. 10, the distributions of tissue displacements in direction z obtained for 10 and 60 s from the viscoelastic and the poroelastic 2D simulations are illustrated. Then, in Fig. 11, the changes in displacements versus time at control points obtained for 2D and 3D geometry are compared.

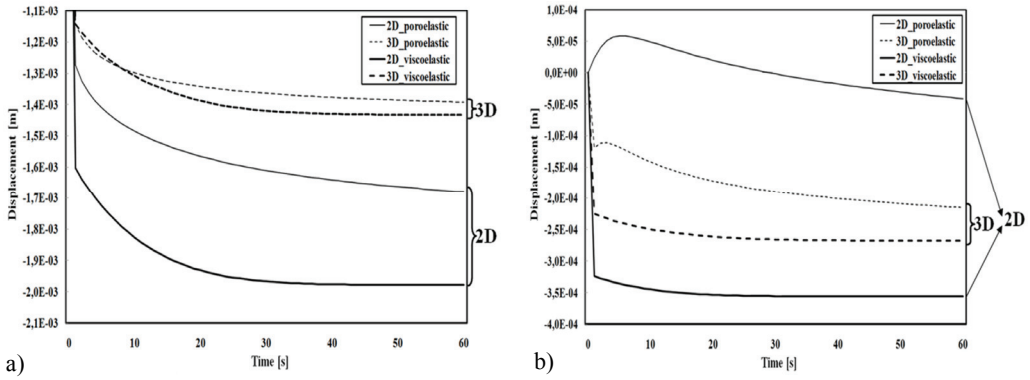

Fig. 11. Comparison of tissue displacement at points G (a) and H (b) for the poroelastic and the viscoelastic models

Large displacements are observed particularly in the vicinity of the loaded region. The spatial changes in displacement both for 10 and 60 s are less significant for the viscoelastic model than for the poroelastic model (Fig. 10). Despite the same elastic properties the model predictions for time evolution of displacement for 2D and 3D geometry visibly diverge (Fig. 11). The displacements at points H and G differ by one order of magnitude.

4. Discussion

Studies of deformation of skinfold under loading of caliper tips (Fig. 3–5) have shown that the shape of creep curves and the creep measure assumed in [11] which is the difference between thickness of loaded tissue at 60 s and 10 s are sensitive to material properties of the viscoelastic and poroelastic models. The form and rate of creep curves obtained from both models are similar when changing the stiffness, Fig. 3. However, when changing the permeability and relaxation time (factors responsible for creep) the form of time dependence of displacement becomes different, Fig. 4. The mechanisms of internal viscous friction of solid (included in the viscoelastic model) and viscous interaction of pore fluid with porous solid skeleton (included in the poroelastic model) cause visibly different time behavior of deformation of the skinfold. While the clinical results obtained in [11] have shown that the creep rate can be a quantitative measure being descriptor of tissue's state, more sensitive than the skinfold thickness, the results of our simulations can confirm this behavior only in the case of short relaxation time, Fig. 5. When the relaxation time of the viscoelastic model of normal tissue amounts to 3 s or less the creep rate predicted by the poroelastic model of tissue, referred to its edematous state, is significantly larger in comparison with the values obtained from the viscoelastic model. When the relaxation time is longer the creep rate appears to be not a good indicator of edema. This may justify the fact of limited application of the diagnostic idea proposed in [11] in clinical practice. The doubts have also found confirmation in results of relatively large set of tests performed in [9]. It should be noticed that the predicted differences of the forms of dependence of deformation of skinfold on time (compare results in Fig. 5) are not fully represented by the creep rate parameter considered and another more appropriate descriptor should be searched to express the discrepancies.

Although the geometry of skinfold and caliper's tips may suggest that 2D geometry of the problem could be a good approximation the results of simulations have proven significant quantitative differences between predictions for 2D and 3D cases. The results for 2D geometry, however, are useful to explain detailed physical phenomena associated with the macroscopic response of the skinfold.

The above results and features of the models considered are significant from diagnostic viewpoint if the models and contributing mechanisms are well recognized and the range of material parameters properly selected for the real human tissues in normal and edematous state. Although in the literature (see the review paper by Wiig and Swartz [14]) the number of factors characterizing complex structure of the tissues are discussed, e.g., interstitial fluid content, structure of colla-

gen and elastin fibers, structure of skin, presence or absence of the lymphatic vessels, etc., up to date detailed mechanisms responsible for the observed behavior of mechanically loaded tissues (including creep) are not fully understood and corresponding macroscopic models not validated. Due to the deficiency of data on human lymphedematous tissue in different pathophysiological stages, such as stiffness or hydraulic conductivity, the possibilities of developing reliable simulations of the tissue behavior are limited.

The results of simulations performed cannot be compared directly to the available clinical data because due to limitation used to apply the linear models the loads in our simulations were almost five times lower than assumed in studies in vivo. Taking into account the advantages of linear modeling (validity of superposition principle) the appropriate methodology of testing in vivo with much lower loading level should be considered as the alternative to use the currently accepted loads and models within large deformation range.

5. Conclusions

The simulations of skinfold under the load of modified Harpenden caliper were elaborated. The predictions of the linear viscoelastic and poroelastic models were compared for 3D and 2D geometry. The time evolution and spatial distributions of tissue displacement, pore fluid pressure and pore fluid velocity were analyzed.

The results of parametric studies show that the form of creep curves and the creep rate predicted by the models considered depend on tissue's stiffness and factors responsible for internal friction (relaxation time or permeability). In the light of the simulations the creep rate parameter defined in [11] appeared to have limited value as the indicator of edema. This is only possible in cases when normal tissues described within the viscoelastic model have very short relaxation time. The viscoelastic model does not deliver explanation of specific creep behavior while the same effects seen in terms of the poroelastic model of tissue can be better physically understood taking into account the pore fluid displacement and pressure dissipation. The discrepancies of predictions for 2D and 3D models are significant and this means that the former one can be only a rough approximation of the process considered.

The understanding of the hydro-mechanical behavior of edematous tissue of skinfold under load can be used in the development of testing methodology and measuring devices. The size and shape of caliper's tips, the time of observations and other parameters could be optimized. Further modeling studies of the skinfold creep should incorporate large deformation range and loads corresponding to the values applied in diagnostic tests.

Acknowledgements

This work was partially supported by the National Science Centre in Poland under grant 2011/01/B/ST8/07283.

References

[1] ARMSTRONG C.G., LAI W.M., MOW V.C., *An Analysis of the Unconfined Compression of Articular Cartilage*, J. Biomech. Eng., 1984, Vol. 106(2), 165–173.

[2] BANKS H.T., HU S., KENZ Z.R., *A Brief Review of Elasticity and Viscoelasticity for Solids*, Adv. Appl. Math. Mech., 2011, Vol. 3, 1–51.

[3] BATES D.O., LEVICK J.R., MORTIMER P.S., *Quantification of rate and depth of pitting in human edema using an electronic tonometer*, Lymphology, 1994, Vol. 27, 159–172.

[4] BIOT M.A., *General theory of three – dimensional consolidation*, J. Appl. Phys., 1941, Vol. 12, 155–164.

[5] DETOURNAY E., CHENG A.H.D., *Fundamentals of poroelasticity*, Chapter 5 in *Comprehensive Rock Engineering: Principles, Practice and Projects, Analysis and Design Method*, C. Fairhurst (ed.), Pergamon Press, 1993, Vol. II, 113–171.

[6] GEERLIGS M., *A literature review of the mechanical behavior of the stratum corneum, the living epidermis and the subcutaneous fat tissue*, Technical Note 2006, PR-TN2006/00450, Koninklijke Philips Electronics N.V.

[7] KACZMAREK M., OLSZEWSKI W.L., NOWAK J., ZALESKA M., *The hydromechanics of edema fluid in lymphedematous lower limb during intermittent pneumatic compression*, Lymphatic Research and Biology, 2015, DOI: 10.1089/lrb.2013.0047.

[8] KACZMAREK M., SUBRAMANIAM R.P., NEFF S.R., *The hydromechanics of hydrocephalus: Steady-state solutions for cylindrical geometry*, Bull. Math. Biol., 1997, Vol. 59, 295–323.

[9] NOWAK K., *Evaluation of axillary fold edema in women with breast cancer according to chosen clinical agents*, PhD Thesis, Nicolaus Copernicus University, Poland, 2014.

[10] OLSZEWSKI W.L., *Physiology – lymph flow, in Lymphedema. A concise compendium of theory and practice*, B.B. Lee, J. Bergan, S.G. Rockson (eds.), Springer 2011, Chap. 9.

[11] ROBERTS C.C., LEVICK J.R., STANTON A.W.B., MORTIMER P.S., *Assessment of truncal edema following breast cancer treatment using modified harpenden skinfold calipers*, Lymphology, 1995, Vol. 28, 78–88.

[12] SMITH J.H., HUMPHREY A.C., *Interstitial transport and transvascular fluid exchange during infusion into brain and tumor tissue*, Microvascular Research, 2007, Vol. 73, 58–73.

[13] STANTON A.W.B, BADGER C., SITZIA J., *Non-invasive assessment of the lymphedematous limb*, Lymphology, 2000, Vol. 33, 122–135.

[14] WIIG H., SWARTZ M.A., *Interstitial fluid and lymph formation and transport: physiological regulation and roles in inflammation and cancer*, Physical Rev., 2012, Vol. 92, 1005–1060.